IEEE Access
Multidisciplinary | Rapid Review | Open Access Journal

Received April 19, 2022, accepted May 3, 2022, date of publication May 9, 2022, date of current version May 13, 2022.

*Digital Object Identifier 10.1109/ACCESS.2022.3173254*

# Camera-Based Channel Modeling and Symbol Error Rate Analysis of CSK Modulation for Outdoor OCC Systems

**KE DONG, XIZHENG KE, (Member, IEEE), AND HUI LI**
School of Automation and Information Engineering, Xi'an University of Technology, Xi'an 710048, China

Corresponding author: Ke Dong (kedong@xaut.edu.cn)

This work was supported in part by the Ph.D. Research Startup Foundation of Xi'an University of Technology under Grant 103-451119004, and in part by the National Natural Science Foundation of China under Grant 61901364.

**ABSTRACT** A camera with an image sensor is an important alternative device to a photodiode-based receiver of visible-light communication in outdoor scenarios. The intrinsic color separation capability of a camera qualifies color shift keying (CSK) modulation as an intuitive solution to enhance the achievable data rate. The symbol error rate (SER) of CSK modulation is considerably important to system design and performance evaluation, and has not been extensively investigated for outdoor optical camera communication systems from the viewpoint of camera-based channel and image processing-based demodulation. In this study, a two-level channel model is proposed to characterize CSK transmission in a single pixel and in the entire image. A general framework of SER analysis for arbitrary CSK constellations was proposed by directly calculating the upper bounds from the empirical distribution of the noise light in the CIE 1931 color space. Through numerical simulations, the influence of the image detector on CSK demodulation was evaluated. The results indicated that an accurate target region is important for maintaining the SER, and an enlarged target region is beneficial when the maximum ratio combination and selective combination algorithms are used in pixel combination.

**INDEX TERMS** Color shift keying, image detector, optical camera communication, pixel combination, symbol error rate, visible light communication.

## I. INTRODUCTION

Optical camera communication (OCC) is a type of visible-light communication (VLC) that uses a camera with an image sensor (IS) as the receiver [1]. Compared to the traditional VLC system based on a photodiode (PD) receiver, OCC has several unique advantages [2]. First, the system implementation is simple because of the highly integrated photodetection chains corresponding to the pixels in the IS. Second, a camera is used in most smart devices, such as smartphones, automobiles, and intelligent home kits; therefore, a general-purpose device with a camera could be fabricated as a receiver of the OCC system. In addition, through image processing, noise light sources can be effectively suppressed in the receiver owing to the spatial separation capability of the IS, which qualifies OCC as a feasible option in outdoor communication environments with strong and dynamic noise lights, similar to the case of vehicle-to-infrastructure, vehicle-to-vehicle, vehicle-to-pedestrian (V2X) communication scenarios [4].

However, OCC has a low transmission rate compared with the PD-based VLC system [3]. In an OCC system, because the transmitted information emitted by the light source is captured by a camera as a series of images and recovered from the pixel states in each image frame (i.e., color and intensity), the data transmission rate is determined by multiplying the information carried in each image frame by the frame rate. For example, the transmission rate is typically 30 to 60 bps for a typical OCC system composed of a white light-emitting diode (LED) light source using undersampled modulation and a complementary metal-oxide-semiconductor (CMOS) IS receiver with a low frame rate [5]–[7]. Therefore, typical manners to increase the transmission rate of OCC are (1) increasing the amount of information carried by each image frame and (2) increasing the IS frame rate. In fact,

The associate editor coordinating the review of this manuscript and approving it for publication was Qinghua Guo.

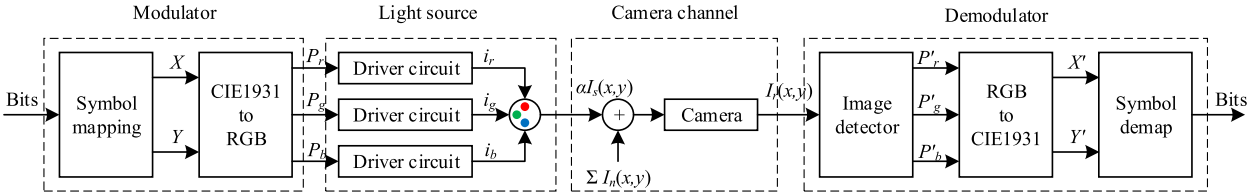


**FIGURE 1.** Transceiver structure of OCC system using CSK modulation.

because the frame rate is largely limited by the imaging hardware, adopting a high IS frame rate, such as a charge-coupled device (CCD), significantly increases the system cost, which eliminates the advantages offered by the camera receiver [8]. For the intensity modulation and direct detection nature of VLC, another manner to increase the data rate is to use $m$-ary modulation schemes on the basis of on-off keying modulation, among which a viable option is color-shift keying (CSK) modulation [9]. In CSK, the data bits modulate the color of the light source at the transmitter to form a CSK symbol corresponding to one of the constellation points and are recovered from the pixel color output by the IS. Owing to the inherent color separation capability of the IS, CSK modulation is preferable in OCC system.

Compared with the indoor scenario, the outdoor environment is more difficult to address for VLC systems because of the strong ambient light and dynamic background noise [10]–[12]. Owing to its spatial and wavelength separation capabilities, the OCC system using CSK modulation plays an important role in noise suppression and data rate enhancement in outdoor V2X communications [13], [14].

In the literature, the system design and performance analysis of CSK have been extensively investigated in VLC systems. The CSK modulation was adopted and recommended as a high-speed PHY specification in the IEEE 802.15.7 standard for VLC [15]. In this specification, 4-, 8-, and 16-CSK constellations were designed within a triangular area based on the International Commission on Illumination (CIE) 1931 color space. Each constellation point represents a 2-, 3-, or 4-order data symbol by emitting different colored lights in the visible light spectrum. In addition, the structures of a red-green-blue (RGB) LED-based modulator and a triple-PD-based demodulator are also suggested. Bai *et al.* optimized the power weight combination group of an RGB LED light source and calculated the symbol error probability for a certain constellation distribution [16]. Singh *et al.* proposed an enhanced CSK modulation scheme using a four-color basis. The resulting symbol error rate (SER) was first approximated for PD-based VLC systems [17]. Based on the four-color constellation design of CSK modulation, Liang *et al.* proposed to transform the color rendering index requirement into a set of linear constraints on a LED source composition to enhance the minimum pairwise Euclidean distance for communication performance optimization [18]. With the assumption of additive Gaussian noise, Jia *et al*. derived an exact SER expression for CSK modulation by converting the three-dimensional (3-D) space of RGB signals to a two-dimensional (2-D) graphically symmetric space [19]. Using a similar method of conversion from 3-D to 2-D signal spaces, Tang *et al.* investigated the exact bit error rate (BER) performance of CSK modulation in a direct manner instead of deriving from SER [20]. Ndjiongue *et al.* presented an analysis of hybrid phase shift keying-color shift keying systems in the hue-saturation-value color space under the additive white Gaussian noise model [21] and proposed a design framework consisting of a mapping technique using amplitude phase shift keying and CSK based on the kite and color wheel structure [22]. In 2019, Halawi *et al.* extended the performance analysis from a PD-based VLC system to an OCC system, using a camera as the receiver [23]. In [23], noise lights with different spatial distributions within pixel coordinates were considered in a 2-D camera-based channel model of OCC, similarly to [24], which was different from that in the PD-based VLC mentioned in the existing literature.

However, most existing performance analyses on the SER or BER of CSK in the literature were performed for a traditional VLC system using a single PD as the receiver. Although the transmitters are interchangeable, two major differences make the existing conclusions inapplicable when a camera with an IS is used as the receiver. First, the channel model is 2-D instead of one-dimensional (1-D). The IS can be regarded as a dense 2-D array of photodetectors that contains a number of independent and integrated photodetection chains (including a photodetector, trans-impendent amplifier, and analog-to-digital converter). Each output is a digitalized light intensity vector in terms of red, green, and blue components corresponding to a pixel in the output image. Second, the spatial distribution of background noise should be well modeled, and the impact on the signal light should be considered in the performance analysis, while the additive white Gaussian noise is insufficient. Therefore, for outdoor OCC systems, the camera-based channel should be modeled in both pixel and image levels to simultaneously characterize the noise effect on signal light reception in each pixel and the array processing against noise light distributed in the image.

The existing investigations of OCC systems have laid a solid foundation for optical camera channel modeling and performance analysis of a specific CSK modulation scheme when a camera is used as the receiver. Although a closed form of the error probability has been derived for specific CSK constellation designs, a general SER analysis for an arbitrary

CSK constellation has not been fully investigated. In addition, the impact of the spatial relationship between pixels (or image processing) on CSK performance has not been well studied.

Based on existing research, the contributions of this study are as follows:

(1) A two-level camera-based channel model was developed for an outdoor OCC system using CSK modulation. At the pixel level, a general noise light with a random color was considered, and the noise effect on the CSK demodulation was represented by a linear deviation of coordinates in the CIE 1931 color space. At the image level, the spatial distributions of the signal light and noise light were considered in pixel coordination under the constraints of the camera parameters;

(2) A general performance analysis framework for arbitrary CSK constellations was proposed by calculating the upper bound of the SER based on the empirical distribution of the Euclidean distance between the signal light and noise light in the CIE 1931 color space;

(3) The influence of multipixel processing in the image detector on the SER was investigated through numerical simulations. The results showed that accurate detection of the target region is considerably significant for maintaining the SER performance, and an enlarged size of the target region only benefits the maximum ratio combination (MRC) and selective combination (SC) algorithms.

The remainder of this paper is organized as follows. Section II describes the typical structure of the camera CSK transceiver. Section III elaborates on the channel model from the single-pixel and multipixel levels. Then, the structure model of the image detector is detailed in Section IV before the derivation of the SER in Section V. Numerical simulation results are presented in Section VI, and Section VII concludes this paper.

## II. TRANSCEIVER STRUCTURE OF CAMERA-CSK

A typical transceiver structure for CSK modulation and demodulation using an RGB LED as the light source and a camera as the receiver is shown in Fig. 1. As a convention, the color coordinates in the CIE color space are represented in uppercase letters, whereas the pixel coordinates are represented in lowercase letters.

### A. CSK MODULATOR

The modulator maps a stream of data bits to CSK symbols according to constellations designed as coordinates (X, Y) in the CIE 1931 color space [15]. The symbol set of $m$-CSK modulation is denoted by $A = \{s_1, s_2, \ldots, s_m\}$, where $s_i = (X_i, Y_i)$ represents the coordinates of each CSK constellation defined in the CIE 1931 color space. For example, the coordinates of IEEE 4-, 8-, and 16-CSK constellations are shown in Fig. 2.

Because each transmitted CSK symbol is conveyed by emitting visible light with a specific wavelength from an RGB LED light source, a CSK symbol $s$ is converted into a normalized power vector to drive the RGB LED by

$$P = \begin{bmatrix} P_R \\ P_G \\ P_B \end{bmatrix} = \mathbf{M}^{-1} \begin{bmatrix} X \\ Y \\ 1 \end{bmatrix}, \tag{1}$$

where $P_R$, $P_G$, and $P_B$ are the power components for red, green, and blue LEDs, respectively, under the total power constraint $P_t = P_R + P_G + P_B$, and $\mathbf{M}$ is the transformation matrix defined as:

$$\mathbf{M} = \begin{bmatrix} x_i & x_j & x_k \\ y_i & y_j & y_k \\ 1 & 1 & 1 \end{bmatrix}, \tag{2}$$

where the pairs $(x_i, y_i)$, $(x_j, y_j)$, and $(x_k, y_k)$ are the coordinates of the center wavelength of the chosen basic color band combinations, i.e., $i$, $j$, and $k$, respectively, which are defined in the CIE 1931 color space. In the IEEE 802.15.7 standard, several sets of basic color band combinations are defined using their center wavelength. For the same band combination, several sets of coordinates for the basic colors are defined. Since this study is independent of a specific CSK constellation design, a typical basic color band combination $(i, j, k) = (110,010,000)$ was chosen for illustration without loss of generality. The corresponding center wavelengths and coordinates of the red, green, and blue basic colors are listed in Table 1.

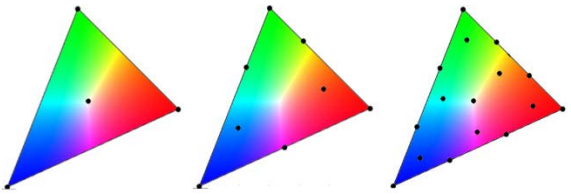


**FIGURE 2.** IEEE 802.15.7 standard (IEEE) constellation sets, (a) 4-CSK, (b) 8-CSK, and (c) 16-CSK.

**TABLE 1.** Coordinates and wavelengths of basic color band combinations (110,010,000) in IEEE 802.15.7 standard [15].

| Band | Color | Center wavelength | (x, y) |
|---|---|---|---|
| $i$ | Red | 753 nm | (0.734, 0.265) |
| $j$ | Green | 509 nm | (0.011, 0.733) |
| $k$ | Blue | 429 nm | (0.169, 0.007) |

### B. LIGHT SOURCE

The light source comprises a LED with independent red, green, and blue channels, and the corresponding driver circuits that function as linearly controlled constant-current sources. The color of the emitted light is determined by the generated driving currents $i_R$, $i_G$, and $i_B$, which are positively proportional to the elements of the input power vector $P$

$$i_c \propto P_c, \quad c \in \{R, G, B\}. \tag{3}$$

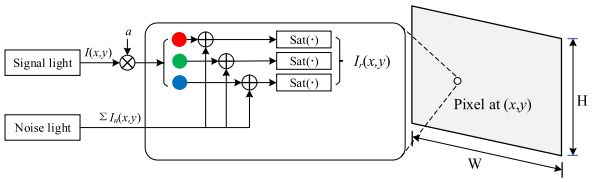


**FIGURE 3.** Model of camera-based channel for CSK modulation.

Note that with the normalized power vector, the total driving current, or the illumination level, is maintained constant owing to the linearity of the driver circuits, which guarantees the dimming condition in the VLC.

### C. CAMERA-BASED CHANNEL

The camera is used in OCC as a 2-D photodetector with each pixel in the IS outputting a digitalized measurement of the light intensities from red, green, and blue channels at a specific coordination, called pixel coordination. In addition to the intended signal light, other unwanted noise lights, such as sunlight, illumination, and billboards, can also be captured by the same camera, which interferes with the signal light reception and degrade CSK demodulation. As shown in Fig. 3,

$$\mathbf{I}_{H\times W} = [I_r(x,y)], \quad x \in [1,H],\ y \in [1,W] \tag{4}$$

denotes the image output by the IS, which contains a 2-D array of pixels with $H$ rows and $W$ columns. When an image frame is output in the RGB format, the captured light intensity for each pixel with coordinates $(x, y)$ is a vector containing the quantified values for the red, green, and blue channels, respectively, as

$$I_r = [I_{r,R}, I_{r,G}, I_{r,B}]^T, \tag{5}$$

where coordinates $(x, y)$ are omitted for simplicity. The color of the received light is determined by the relative intensities of the RGB components. Thus, the pixel color in the output image differs from the color of the light source if one or more noise light sources interfere with the signal light at the same pixel by adding an effective noise RGB vector upon the received signal light. Generally, since the noise light source has a wide spectrum beyond the image sensors detection range (e.g., sunlight), an effective noise light is assumed with a wavelength within the detection range of the IS. In addition, the crosstalk between RGB channels, which exists in practical IS detection, can be suppressed by channel estimation. Since channel estimation is beyond the scope of this paper, the crosstalk effect is neglected in Fig. 3 for simplicity. The detailed camera-based channel model and noise model are described in Section III.

### D. IMAGE DETECTOR

Because the purpose of the demodulator is to determine the transmitted symbol from the output images captured by the camera, an image detector is required to find the received color of the signal light, represented by a normalized RGB intensity vector $\bar{P}$, according to the received image data $\mathbf{I}_{H\times W}$. Therefore, the image detector combines the colors of the image pixels into an "effective" color, which can be modeled as a transformation $F_{ID}$, that is

$$\bar{P} = [\bar{P}_R, \bar{P}_G, \bar{P}_B]^T = F_{ID}(\mathbf{I}_{H\times W}), \tag{6}$$

under the total intensity constraint

$$\bar{P}_R + \bar{P}_G + \bar{P}_B = P_r. \tag{7}$$

In practice, to reduce the computation overhead, the image detector is generally implemented using target area detection prior to pixel combination. Target detection is used to determine a subset of pixels in the output image (or target region) that covers the intended signal light source. Then, the effective color vector $\bar{P}$ is generated by combining the colors of these pixels in the subset using different combining techniques such as equal gain combination (EGC), MRC, and SC. However, beyond the scope of this paper, more than one target area can be detected simultaneously by image detection, which is useful in multiple-in multiple-out processing, particularly for vehicular VLC systems using a pair of headlights or taillights as the transmitter [25], [26], [30]. The image detector model is described in detail in Section IV.

### E. SYMBOL DETECTION

Because the color of each signal light is detected as an RGB power vector $\bar{P}$, the received light point $p_r$ in the CIE 1931 color space is obtained using the inverse version of (1) as

$$p_r = \begin{bmatrix} X_r \\ Y_r \\ 1 \end{bmatrix} = \frac{1}{P_r}\mathbf{M}\bar{P}, \tag{8}$$

where $1/P_r$ is the normalization factor of $\bar{P}$.

In practice, with the impact of noisy light, the color of the received light may be slightly different from that of the light source, which is equivalent to $p_r$ deviating from the transmitted CSK constellation point $s$ in the CIE 1931 color space. Therefore, when an equiprobable constellation is employed, the maximum-likelihood (ML) decision criterion is equivalent to finding the transmitted CSK symbol as the constellation point with the minimum Euclidean distance to the received point, that is

$$\widehat{p} = \arg\min_{s_i \in A} \|p_r - s_i\|. \tag{9}$$

Note that the third element in vector $p_r$ is omitted for simplicity.

## III. CAMERA-BASED CHANNEL MODEL

From the transceiver structure of camera-CSK shown in Fig. 1, each pixel of the IS in the camera can be regarded as an independent photoelectric detection chain, and the image is the output from a 2-D array of photoelectric detectors. Through the image detector, the image with 2-D information is converted into an RGB intensity vector for output, upon

which the transmitted CSK symbol is determined and recovered from the impacts of noisy light.

The transmission channel can be modeled using two levels. The base level is the single-pixel model, which is similar to the traditional single-PD receiver, neglecting the spatial distribution of the signal and noise lights on the photosensitive surface. The top level is the multipixel model, which describes the spatial distribution of signal light and noise light based on the single-pixel model and enhances the demodulation performance while realizing dimensionality reduction through image processing.

### A. SINGLE-PIXEL MODEL

As observed in Fig. 1, the modulation, transmission, and demodulation of a camera-CSK symbol occur in the following two spaces:

(1) Color spaces. At the transmitter, the CSK constellation points correspond to the 2-D coordinates defined in the CIE 1931 color space. According to the coordinates, the currents to drive the red, green, and blue LEDs in the RGB light source are generated to compose the emitting light with a specified color in the RGB color space. At the receiver, the IS restores the RGB components of the light sensed by the pixels in the RGB color space, and converts them to the CIE 1931 color space coordinates before symbol decision and data demodulation

(2) Pixel space. After emitted by the light source, the signal light arrives at the photosensitive surface of the IS through free space propagation and is superimposed by the noise light. According to the spatial distribution of signal light and noise light, different illuminations are produced on the pixels at different positions, which accounts for a projection of the spatial distribution of the light intensity in the pixel space.

From the perspective of the channel model, the interference of the noise light to the signal light occurs in the pixel space, but its influence on the CSK symbol demodulation is reflected in the color spaces (i.e., RGB and CIE 1931 color space). Therefore, we translated the influence of noise light on signal light into CIE 1931 color space for analysis, and established a single-pixel channel model as shown in Fig. 4.

In the model shown in Fig.4, each light is represented by a triple $(X, Y, P)$, where $(X, Y)$ represents the coordinates of the signal light in the CIE 1931 color space, corresponding to the color of the signal light, and $P$ is the intensity (or power) of the light. For example, $S(X_s, Y_s, P_T)$ represents the transmitted signal light emitted by the light source, the coordinates of its color in the CIE 1931 color space are $(X_s, Y_s)$, and the total emission power is $P_T$. After propagation in free space, the signal light received by a pixel on the IS photosensitive plane is denoted by $S'(X_s, Y_s, aP_t)$, which the transmitted signal light because the received signal light experiences a path loss of $a$ to the light intensity but maintains the color because the relative intensities of the RGB channels remain unchanged. Similarly, we denote $N(X_n, Y_n, P_n)$ as the noise light received by this pixel and $S_r(X_r, Y_r, P_r)$ as the received light used for

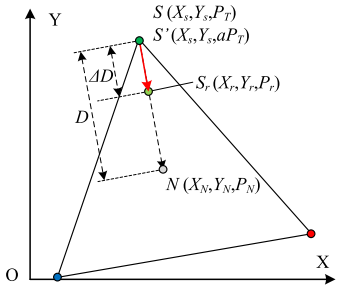


**FIGURE 4.** Single-pixel channel model in CIE 1931 color space. The color of the received light $S_r$ is a linear deviation away from signal light $S$ and $S'$ towards the color of noise light $N$ in distance $D$ by $\Delta D$.

demodulation, and the following relationship is satisfied

$$\begin{bmatrix} X_r \\ Y_r \\ 1 \end{bmatrix} = \frac{1}{P_r}\mathbf{M}\begin{bmatrix} a\bar{P}_R + P_{n,R} \\ a\bar{P}_G + P_{n,G} \\ a\bar{P}_B + P_{n,B} \end{bmatrix}, \tag{10}$$

where $P_{n,R}$, $P_{n,G}$, and $P_{n,B}$ are the RGB components of the noisy light under the total intensity constraint $P_{n,R} + P_{n,G} + P_{n,B} = P_n$, $a$ is the pass loss factor of line-of-sight propagation, and $P_r = aP_t + P_n$ is the received light intensity.

Using (8) into (10), we obtain

$$\begin{bmatrix} X_r \\ Y_r \\ 1 \end{bmatrix} = \frac{aP_T}{aP_T + P_N} \cdot \frac{1}{P_T}\begin{bmatrix} P_R \\ P_G \\ P_B \end{bmatrix} + \frac{P_N}{aP_T + P_N} \cdot \frac{1}{P_N}\begin{bmatrix} P_{n,R} \\ P_{n,G} \\ P_{n,B} \end{bmatrix}. \tag{11}$$

Denoting $\rho = \frac{aP_T}{P_N}$ as the signal-to-noise ratio (SNR), we obtain

$$\begin{bmatrix} X_r \\ Y_r \\ 1 \end{bmatrix} = \frac{\rho}{1+\rho}\begin{bmatrix} X_s \\ Y_s \\ 1 \end{bmatrix} + \frac{1}{1+\rho}\begin{bmatrix} X_n \\ Y_n \\ 1 \end{bmatrix}. \tag{12}$$

As shown in Fig. 4, the coordinates of the received light in the CIE 1931 color space are a linear combination of those of the signal and noise lights. In other words, although the signal light is superimposed on the noise light in the pixel space, the noise impact in the CIE 1931 color space is a linear deviation of the received signal point away from the constellation point towards the noise point (i.e., from $S'$ to $S_r$). The amount of deviation depends on the distance and intensity ratio between the signal and noise lights. Therefore, $D$ denotes the Euclidean distance between points $S'$ and $N$ as follows

$$D = \sqrt{(X_s - X_n)^2 + (Y_s - Y_n)^2}. \tag{13}$$

This is a measurement of the color difference between the signal light and noise light, and the linear deviation of the color of the signal light caused by additive noise can be measured by the distance between $S'$ and $S_r$, that is, $\Delta D = \sqrt{(X_s - X_r)^2 + (Y_s - Y_r)^2}$. Using (12), we obtain

$$\Delta D = \frac{D}{1+\rho}. \tag{14}$$

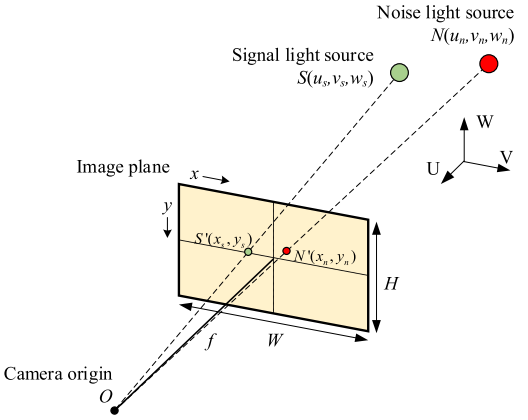


**FIGURE 5.** Perspective projection of signal and noise light sources.

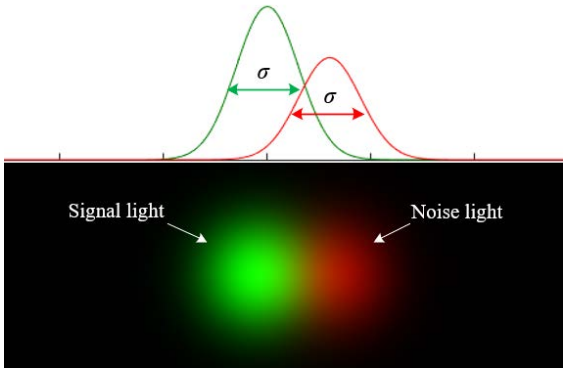


**FIGURE 6.** Image blurring model based on 2-D Gaussian functions.

### B. MULTI-PIXEL MODEL

In contrast to PD-based VLC, OCC uses a camera as the receiver, which leads to a 2-D channel composed of a 2-D array of single-pixel models. A typical camera comprises an IS that converts the light intensities received by each pixel into a 2-D data structure (i.e., image) and an optical lens to control the field of view. Essentially, the channel model of an OCC is an imaging process that projects a 3-D space into a 2-D plane. Therefore, the structural parameters of the camera were incorporated into the channel modelling process.

As shown in Fig. 5, denoting $S(u_s, v_s, w_s)$ and $N(u_n, v_n, w_n)$ as the signal and noise source in world coordination, and the center positions in pixel coordination as $S'(x_s, y_s)$ and $N'(x_n, y_n)$, respectively, the transformation is [27]

$$\begin{bmatrix} \tilde{x}_s \\ \tilde{y}_s \\ \tilde{z}_s \end{bmatrix} = \begin{bmatrix} 1/\rho_x & s_o & o_x \\ 0 & 1/\rho_y & o_y \\ 0 & 0 & 1 \end{bmatrix} \begin{bmatrix} f & 0 & 0 & 0 \\ 0 & f & 0 & 0 \\ 0 & 0 & 1 & 0 \end{bmatrix} \times \begin{bmatrix} \mathbf{R}_{3\times3} & \mathbf{t}_{3\times1} \\ \mathbf{0}_{1\times3} & 1 \end{bmatrix} \begin{bmatrix} u_s \\ v_s \\ w_s \\ 1 \end{bmatrix}, \quad (15)$$

where $(\tilde{x}_s, \tilde{y}_s, \tilde{z}_s)$ is a homogeneous representation of the pixel $S'(x_s, y_s)$. $\rho_x$ and $\rho_y$ are effective pixel sizes defining the aspect ratio of the captured image, and $s_o$ is the skew parameter describing any non-orthogonality between the image axes. $(o_x, o_y)$ is the image center or principal point, and $f$ is the focal length. $\mathbf{R}$ and $\mathbf{t}$ are the rotation matrix and the translation vector, respectively.

In addition to the image position, these parameters also determine the image size of the light sources (i.e., signal and noise lights) in the number of pixels as in [28]

$$l = \frac{fl'}{de}. \quad (16)$$

This indicates that for a light source with dimension $l'$ at distance $d$, the image size in pixel $l$ is proportional to the focal length of the camera $f$ with respect to the pixel size $e$.

Because of the blurring effect of the IS during imaging, as shown in Fig. 6, the brightness distribution of the light source in the image is not abrupt but expands slowly and smoothly around the center position. Such a blurring effect can be modeled as a 2-D Gaussian function as [29]

$$I(x, y) = I_0 \exp\left(-\frac{(x - x_0)^2 + (y - y_0)^2}{2\sigma^2}\right), \quad (17)$$

where $(x_0, y_0)$ is the center position of the light source in the image and $I_0$ and $\sigma$ are the intensity and standard deviation, respectively, depending on the distribution of the light source, such as the size, radiation pattern, direction, distance, and intensity. Simultaneously, the saturation effect of IS produces brightness clipping on pixels whose intensity exceeds a certain threshold.

### C. CAMERA-CSK CHANNEL MODEL

From the single-pixel and multi-pixel models mentioned above, the following characteristics can be drawn for the camera-CSK channel model.

In RGB color space, the color of the signal light and noise light can be determined by the relative intensities of the red, green, and blue channels, namely $P$, whereas in the CIE 1931 color space, under a set of selected basic colors, they are represented by coordinate points in 2-D space, namely $p(X, Y)$, In addition, the color of light is assumed unchanged in free space propagation with path loss.

The influence of noise on signal light reception is manifested as a color change. In the RGB color space, this impact is manifested as a superposition of the RGB components, whereas in the CIE 1931 color space, it behaves as a linear deviation of the coordinates of the received light away from the constellation point along the direction of the noise light coordinate point, and the amount of deviation is related to the SNR of the pixel.

The signal and noise lights are received by the photosensitive plane with a 2-D array of pixels, and their intensity distribution can be represented by a 2-D Gaussian function with their position, intensity, and size depending on the light source distribution and camera parameters. The signal light

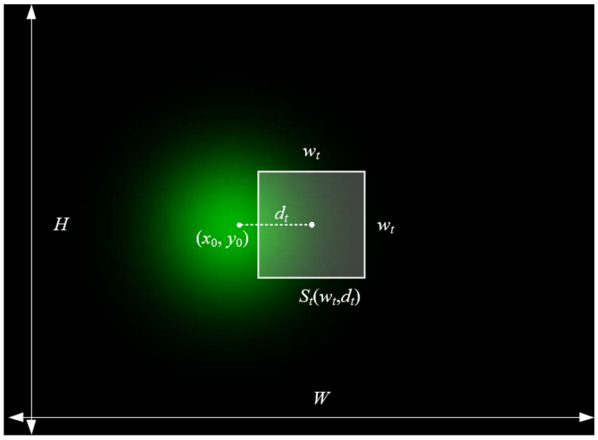


**FIGURE 7.** Square target region with edge length $w_t$ and deviation distance d away from the center of the signal light spot ($x_0$, $y_0$).

intensity and noise light intensity distributions received by each pixel on the IS are related to the light source size, distance, and camera parameters.

## IV. IMAGE DETECTOR

Because the light source is sensed simultaneously by multiple pixels in the IS, the image detector is essentially a color combinator that transforms the pixel colors within the target area into a single-color output, from which the transmitted CSK constellation is determined. As shown in Fig. 7, in an image with a resolution of $H \times W$, a square target region $S_t(w_t, , d_t)$ is defined around the signal light spot by the edge length $w_t$ in the number of pixels and the deviation distance $d_t$ between the centers of the target area and signal light.

Although the detection algorithm of the target region (i.e., region of interest), which has been investigated in the literature on vehicular VLC [30], is beyond the scope of this study, we assume that a single target area is detected and investigate the impacts of the area and deviation distance on the SER performance under different combination algorithms.

Suppose that the general form of image detector is

$$F_{ID}(\mathbf{I}_{H\times W}) = \sum_{(x,y)\in S_t(w_t,d_t)} C(x,y) I_r(x,y), \tag{18}$$

where $I_r(x, y)$ is the RGB vector of pixel color at $(x, y)$ in image $\mathbf{I}_{H\times W}$, and $C(x, y)$ is the combination weight for each pixel. Three combination algorithms are considered in this study, which are EGC, MRC, and SC.

For EGC, $C(x, y) = 1/w_t^2$ is a constant that refers to a pixel-wise average of the colors within the target area.

For MRC,

$$C(x,y) = \frac{\rho(x,y)}{\sum_{(x,y)\in S_t} \rho(x,y)}, \tag{19}$$

where $\rho(x, y)$ is the SNR in pixel $(x, y)$, which indicates that the pixel colors are combined by weighing their SNRs.

For SC,

$$C(x,y) = \delta(x - x_m, y - y_m), \tag{20}$$

where $\delta(x, y)$ is the Dirac function and

$$(x_m, y_m) = \underset{(x,y)\in S_t(w_t,d_t)}{\arg\max}\ \rho(x,y). \tag{21}$$

## V. CALCULATION OF SYMBOL ERROR RATE

### A. UPPER BOUND OF SER FOR CSK

From (11) and (12), a coordinate deviation from the transmitted constellation point caused by noise contamination results in errors in the CSK demodulation. Under the ML criterion, when the received pixel color is too far from the transmitted light color and is more likely to be the color corresponding to another CSK symbol, demodulation error occurs accordingly.

Owing to the irregular shape of the color space determined by the chosen color bands, it is difficult to analytically describe the exact boundaries of the demodulation regions for each constellation point under the ML criterion as well as the SER performance. However, the upper bound of the SER for the $i$-th symbol can be described as:

$$P_{e,i} < \Pr\{\Delta D > \min\{d_{ij}/2\}\}, \quad i, j \in [0, m-1] \text{and} i \neq j, \tag{22}$$

where $\Delta D$ is the deviation distance from the constellation point under the noise light, and $d_{ij}$ is the distance between the $i$-th and $j$-th constellation points in the CIE 1931 color space. This indicates that for each CSK symbol, the error probability is upper bounded by the minimum distance away from other constellations and the distribution of the deviation distance caused by random noise light. Although (13) is difficult to derive because the random variable $\Delta D$ is not a known distribution, we can analyze the upper bound of SER for a specific constellation set as follows:

We assume that the intensities of the basis colors of the noise light are independently, identically, and uniformly distributed random variables with normalized power $P_N$, as defined in (1). This indicates that the noise light for a pixel is a random point uniformly distributed within the entire triangular region defined by the chosen basis color bands.

Suppose that a noisy light with a random color corresponds to a point away from a constellation point with distance $D$. From (11) and (12), it interferes with the signal light and deviates from the constellation point with a distance of $\Delta D = D/(1 + \rho)$; all such noise lights are uniformly distributed on the arc within the triangle region, taking the center as the constellation point and radius $D$. Therefore, the empirical distribution of $\Delta D$ can be substituted by the distribution of the effective arc length with radius $D$. From this point, (13) is equivalent to:

$$P_{e,i} < \Pr\{D > (1 + \rho) \min\{d_{ij}/2\}\} \tag{23}$$

From (23), the upper bound of the SER for the CSK symbol is determined by the following factors:

(1) The color of the noise light, which is represented by the distribution of noise light away from the constellation point in the CIE 1931 color space. Apparently, the assumption of a uniformly distributed RGB color vector of the noise light is equivalent to leading to a uniformly distributed point within the region of the chosen color triangle. Therefore, although the distribution of the distance $D$ from each constellation point is unknown, it has a fixed probability density function (PDF) and cumulative distribution function (CDF) determined by the constellations, which can be obtained by empirical calculations.

(2) Distance between constellation points. Using ML detection criteria, half of the minimum distance $d_{ij}$ from the $i$-th constellation to the others behaves as a threshold to calculate the SER, given the CDF of the noise color distribution. Evidently, the ratio between the signal and noise $(1+\rho)$ is an adjustment factor for the threshold.

### B. EMPIRICAL DISTRIBUTION OF D

Because the noise color is uniformly distributed within the triangle region of the CIE 1931 color space, the empirical PDF and complementary CDF (CCDF) of $D$ with respect to each constellation can be numerically calculated using a statistic of the arc length $arc(D)$. An example of the constellation S0 in 4-CSK is shown in Fig. 8. Using this method, the empirical distribution of $D$ for the IEEE 4-CSK constellations is calculated and is shown in Fig. 9. Note that the distribution of $D$ is dependent only on the constellation design under the assumption of random noise light. Therefore, these calculations can be performed offline.

Using the minimum distance data listed in Table 2 and (14), the upper bound of the SER for the constellation point $S_i$ in IEEE 4-CSK with uniformly distributed color noise light is:

$$\hat{P}_{e,i} = F\left((1+\rho)\min\{d_{ij}/2\}\right), \quad i,j \in [1,m],\ i \neq j, \tag{24}$$

where $F(\cdot)$ is the empirical CCDF of $D$, as shown in Fig. 9. When constellations are transmitted with equal probability, the overall SER is upper bounded by

$$\bar{P}_e = \frac{1}{m}\sum_{i=0}^{m}\hat{P}_{e,i}. \tag{25}$$

## VI. NUMERICAL SIMULATIONS

In this section, numerical simulations of the performance of the SER are conducted at the pixel and image levels. The pixel level is based on the single-pixel model, without considering the spatial distribution of the signal light or noise light in the pixel space. At this level, the upper bound of the SER for each constellation point is calculated under noisy light with a random color, and the gaps between the upper bounds and simulated results are investigated and illustrated in the CIE 1931 color space. The image level is based on a multipixel model with 2-D Gaussian distributed intensities for signal light and random noise light. At this level, the impacts of the area and deviation distance of the target region and the combining algorithm on the SER performance of the image detector were evaluated through numerical simulation.

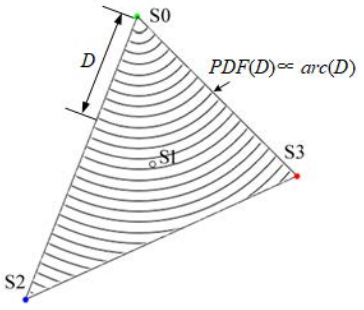


**FIGURE 8.** Illustration of the empirical distribution of $D$ for constellation S0 in IEEE 4-CSK.

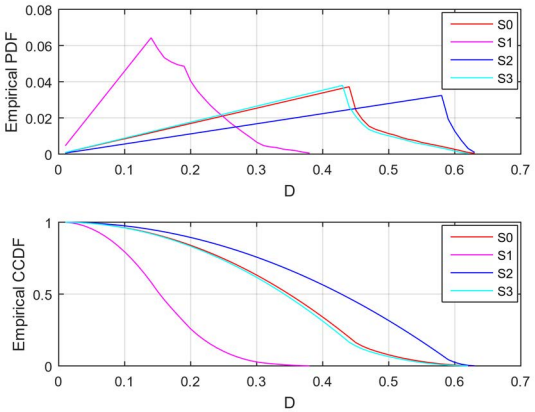


**FIGURE 9.** Empirical PDF and CCDF of D for 4-CSK constellations.

**TABLE 2.** Constellation distance for IEEE 4-CSK.

| $d_{ij}$ | $j=0$ | $j=1$ | $j=2$ | $j=3$ | $\min\{d_{ij}/2\}$ |
|---|---|---|---|---|---|
| $i$=0 | / | 0.3088 | 0.6343 | 0.4695 | 0.1544 |
| $i$=1 | 0.3088 | / | 0.3884 | 0.3000 | 0.1500 |
| $i$=2 | 0.6343 | 0.3884 | / | 0.6211 | 0.1942 |
| $i$=3 | 0.4695 | 0.3000 | 0.6211 | / | 0.1500 |

### A. PIXEL LEVEL

At this level, considering IEEE 8-CSK as an example, we calculated the upper bounds of SER for each constellation point using (24) and obtained the overall performance using (25). In addition, compared with the upper bounds, numerical simulations on SER were performed for IEEE 4-, 8-, and 16-CSK by generating a large number of random CSK symbols with interference by noise light with a random color.

#### 1) UPPER BOUND OF SER

To calculate the upper bound of SER for IEEE 8-CSK, we first obtained the empirical CCDF of deviation distance $D$ for each constellation point with predefined coordinates in the CIE 1931 color space as depicted in Figs. 8 and 9. Then,

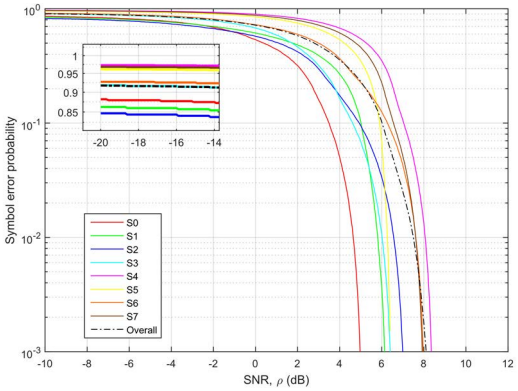


**FIGURE 10.** Upper bounds of SER of each constellation in the IEEE 8-CSK modulation.

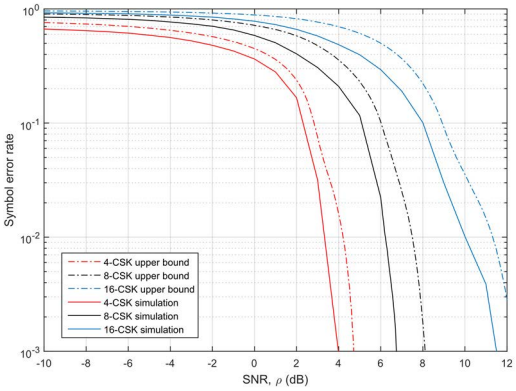


**FIGURE 11.** SER simulation results for IEEE 4-, 8-, and 16-CSK constellations.

the halves of minimum distances (i.e., $\min\{d_{ij}/2\}$) between the constellation points were calculated. Using the CCDF and $\min\{d_{ij}/2\}$ with (24), the upper bound of the SER for IEEE 8-CSK was calculated for each constellation point, as shown in Fig. 10. Moreover, the overall SER performance was determined using (25) under the equiprobable assumption.

Equation (24) indicates that the error probability is upper bounded by the CCDF of $D$ when $D = (1+\rho)\min\{d_{ij}/2\}$, where $\min\{d_{ij}/2\}$ are fixed given a specific constellation design (refer to Table 2 for IEEE 4-CSK). Therefore, as shown in Fig. 10, the upper bounds of SER for each constellation point shrink as the SNR (i.e., $\rho$) increases. However, the interesting part is the difference between the constellations. Evidently, some of the individual constellations (e.g., S0 and S1) exhibited a better SER performance than that in the overall situation with equal probabilities among the constellations. As we known from (23)–(24) and Fig. 9, such a difference, particularly in the high-SNR region, originates from the distribution function of $D$ with a large value. Under the basic assumption of uniformly distributed data bits, an optimization of the constellation design or a weighted decision criterion is suggested to improve the overall SER performance. In addition, in the low-SNR region, there are constant gaps among the constellations, which indicates that even if the noise light is strong, an error-free probability exists for each constellation, which varies from the constellations.

### 2) SIMULATION RESULTS

In addition to the calculated upper bounds, the SER was evaluated through simulation in three steps as follows. First, a large number of CSK symbols were generated by selecting from constellations with equal probabilities. Then, a signal light was emitted with a color corresponding to the constellation point within the triangle subregion defined by the red, green, and blue bands in the CIE 1931 color space.

Second, the noise light source was assumed to have a random color corresponding to a point with uniformly distributed random coordinates within the same subregion as the signal light.

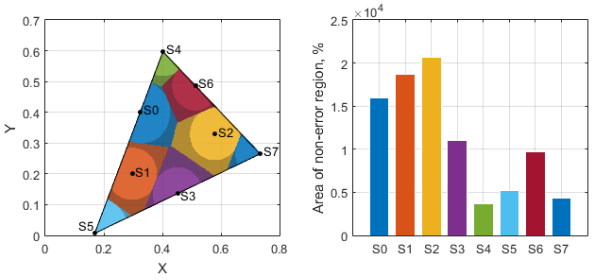


**FIGURE 12.** Decision regions and their areas. (a) Circular decision regions in bright color are used for upper bound calculation and irregular regions in dark color are excluded. (b) Comparison of areas of decision regions in bright color for each constellation.

**TABLE 3.** Simulation parameters.

| Symbol | Name | Value or distribution |
|---|---|---|
| $H\times W$ | Resolution of image sensor | 720×1080 |
| $(x_0, y_0)$ | Center of signal light spot | $(W/2, H/2)$ |
| $\sigma_s$ | Standard deviation in pixels | 30 |
| $I_0$ | Max intensity of signal light | 0.7 |
| $(x_{0,n}, y_{0,n})$ | Center of noise light spot | $\sim\mathbf{U}(1,W)$, $\sim\mathbf{U}(1,H)$, |
| $\sigma_n$ | Standard deviation in pixels | 30 |
| $I_n$ | Max intensity of noise light | Variable |

Third, the receiver (i.e., a pixel in the image) captured a combination of the signal and noise lights with a given SNR $\rho$ and output a color vector with RGB components. The output pixel color was then transformed into a received point in the CIE 1931 color space, and the transmitted symbol was estimated using the ML criteria by determining the shortest Euclidean distance from the received point to the constellation points. Finally, the SER was calculated by comparing the received symbol with the transmitted ones.

Compared with the calculated upper bounds, the simulation results of the SER for different CSK modulations (e.g., IEEE 4-, 8-, and 16-CSK) are shown in Fig. 11. As the modulation order increased, more errors occurred in the symbol decision, owing to the shorter distance between the constellations in the CIE 1931 color space. In addition, a gap was

observed between the simulation results and upper bound for each modulation scheme. This means that the actual decision region where the received light lied around the constellation point in the simulation was larger than that used in the upper-bound calculation in (24). As an explanation, the decision regions are depicted in Fig. 12(a) in different colors for each constellation. Here, the circular regions in bright colors represent the decision regions used in the upper-bound calculations, which are circles with centers at constellation points and radii equal to half of the minimum distance from the constellation to the others (i.e., $\min\{d_{ij}/2\}$). In addition, the irregular regions in dark colors are the actual decision regions excluded from the upper-bound calculations, but included in the simulations.

In fact, because of the linear deviation effect of noise light mentioned in Section III, no error occurred when the noise light fell within the decision region of the transmitted constellation at any SNR, which means that the color of the signal light did not change significantly by noise light with a color similar to that of the signal light. Therefore, the decision region determines the error-free probability for a low SNR. Fig. 12(b) shows the areas of the decision regions in bright color, which illustrates and explains that the constellation with the larger decision region has a lower SER at a low SNR.

### B. IMAGE LEVEL

Simulations were performed at the image level with emphasis on the impact of the image detector on the SER performance. The simulation parameters are listed in Table 3. A camera with an IS and a resolution of 720 p was used as the receiver. It was assumed that the signal light spot had a specific color depending on the modulated CSK symbol, and the light intensity distribution in pixel space was modeled as a 2-D Gaussian function with the center located at the center of the field of view and a standard variance of 40 pixels. In contrast, the noise light spot had a random color and shared the same spatial distribution as the signal light, except that the random center location was uniformly distributed within the 2-D pixel space. In addition, the maximum intensity was fixed as $I_0 = 0.7$ for the signal light but variable as $I_n = I_0/\eta$ for the noise light, where $\eta$ is the effective SNR.

In the image-level simulation, the CSK modulation and demodulation were the same as those performed at the single-pixel level, except for the image detector, where the output image was converted into an ''effective'' pixel by color combination over the pixels within a determined target region. To illustrate the impact of the image detector on SER, using IEEE 16-CSK as an example, Fig. 13 shows the SER performance as the deviation distance between the target region; the signal light spot increased under a moderate noise level $\eta = 1$. In addition, comparisons are provided for different sizes of target regions and the combination algorithms.

The following observations were made: (1) With a fixed size, as the target area deviated from the center of the signal light spot, SER increased accordingly. Such performance degradation accounts for the low accuracy of the target region

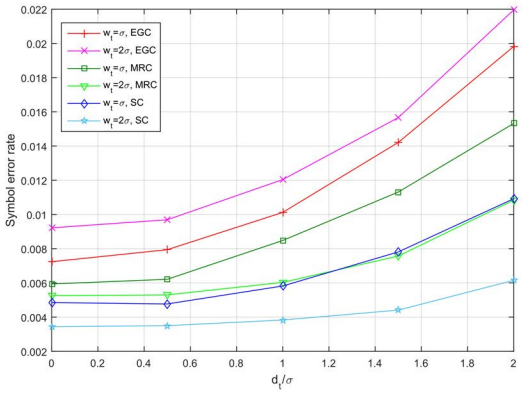


**FIGURE 13.** SER of IEEE 16-CSK modulation with different target region configurations using EGC, MRC, and SC algorithms and given $\eta = 1$.

detection. (2) For pixel combination, compared with the simple EGC algorithm, the SER performance could be improved using sophisticated algorithms (i.e., MRC or SC) that rely on the SNRs on each pixel, which can be regarded as the estimated channel state information (CSI). (3) Without CSI, expanding the size of the target region (i.e., edge length $w_t$ from $\sigma$ to $2\sigma$) does not ensure an improvement (e.g., EGC), but introduces extra noisy pixels. However, when CSI is available, using MRC or SC is more beneficial for an enlarged target region because the high SNR pixels are more likely to be maintained (for SC) or contribute (for MRC) to output the ''effective'' pixel.

## VII. CONCLUSION

In this study, the channel modeling and SER performance were investigated for an OCC system using CSK modulation. By introducing an image detector to the transceiver structure, we proposed a two-level camera-based channel model. At the pixel level, the influence of noise light with a random color was represented by a linear deviation of the coordinates in the CIE 1931 color space. At the image level, the spatial distribution of the received light intensity was considered in pixel space, including the parameters of the camera. Based on the empirical distribution of the Euclidean distance between the signal and noise lights, the upper bound of the SER was calculated using the SNR and the minimum inter-constellation distance as the threshold. Through numerical simulations, the imbalanced SER between the constellations suggested further optimization, and the gaps from the upper bounds were justified and explained by the decision region under the ML criteria. In addition, the simulation results indicated that the accuracy and combination method of the image detector had a significant impact on the SER performance of the OCC system using CSK modulation.

## REFERENCES

[1] W. A. Cahyadi, Y. H. Chung, Z. Ghassemlooy, and N. B. Hassan, ''Optical camera communications: Principles, modulations, potential and challenges,'' *Electronics*, vol. 9, no. 9, p. 1339, Aug. 2020.

[2] X. Li, N. B. Hassan, A. Burton, Z. Ghassemlooy, S. Zvanovec, and R. Perez-Jimenez, "A simplified model for the rolling shutter based camera in optical camera communications," in *Proc. 15th Int. Conf. Telecommun. (ConTEL)*, Jul. 2019, pp. 1–5.
[3] T. Nguyen, A. Islam, M. T. Hossan, and Y. M. Jang, "Current status and performance analysis of optical camera communication technologies for 5G networks," *IEEE Access*, vol. 5, pp. 4574–4594, 2017.
[4] A. Memedi and F. Dressler, "Vehicular visible light communications: A survey," *IEEE Commun. Surveys Tuts.*, vol. 23, no. 1, pp. 161–181, 1st Quart., 2021.
[5] R. D. Roberts, "A MIMO protocol for camera communications (CamCom) using undersampled frequency shift ON-OFF keying (UFSOOK)," in *Proc. IEEE Globecom Workshops (GC Wkshps)*, Dec. 2013, pp. 1052–1057.
[6] P. Luo, Z. Ghassemlooy, H. Le Minh, X. Tang, and H.-M. Tsai, "Undersampled phase shift ON-OFF keying for camera communication," in *Proc. 6th Int. Conf. Wireless Commun. Signal Process. (WCSP)*, Oct. 2014, pp. 1–6.
[7] P. Luo, M. Zhang, Z. Ghassemlooy, S. Zvanovec, S. Feng, and P. Zhang, "Undersampled-based modulation schemes for optical camera communications," *IEEE Commun. Mag.*, vol. 56, no. 2, pp. 204–212, Feb. 2018.
[8] N. T. Le, M. A. Hossain, and Y. M. Jang, "A survey of design and implementation for optical camera communication," *Signal Process., Image Commun.*, vol. 53, pp. 95–109, Apr. 2017.
[9] P. Luo, M. Zhang, Z. Ghassemlooy, H. L. Minh, H.-M. Tsai, X. Tang, L. C. Png, and D. Han, "Experimental demonstration of RGB LED-based optical camera communications," *IEEE Photon. J.*, vol. 7, no. 5, pp. 1–12, Oct. 2015.
[10] A. R. Ndjiongue and H. C. Ferreira, "An overview of outdoor visible light communications," *Trans. Emerg. Tel Tech.*, vol. 29, Jul. 2018, Art. no. e3448.
[11] M. Karbalayghareh, F. Miramirkhani, H. B. Eldeeb, R. C. Kizilirmak, S. M. Sait, and M. Uysal, "Channel modelling and performance limits of vehicular visible light communication systems," *IEEE Trans. Veh. Technol.*, vol. 69, no. 7, pp. 6891–6901, May 2020.
[12] X. Ke, Q. I. N. Huanhuan, Y. A. N. G. Shangjun, W. U. Jiali, and P. A. N. Xiya, "Night background light noise model of visible light communication system in vehicle networking environment," *Chin. J. Radio Sci.*, vol. 36, no. 6, pp. 986–990, 2021.
[13] T. Yamazato, I. Takai, H. Okada, T. Fujii, T. Yendo, S. Arai, M. Andoh, T. Harada, K. Yasutomi, K. Kagawa, and S. Kawahito, "Image-sensor-based visible light communication for automotive applications," *IEEE Commun. Mag.*, vol. 52, no. 7, pp. 88–97, Jul. 2014.
[14] M. K. Hasan, M. O. Ali, M. H. Rahman, M. Z. Chowdhury, and Y. M. Jang, "Optical camera communication in vehicular applications: A review," *IEEE Trans. Intell. Transp. Syst.*, early access, Jun. 16, 2021, doi: 10.1109/TITS.2021.3086409.
[15] *IEEE Standard for Local and Metropolitan Area Networks—Part 15.7: Short-Range Optical Wireless Communications*, Standard802.15.7-2018, Apr. 2019, pp. 1–407.
[16] B. Bai, Q. He, Z. Xu, and Y. Fan, "The color shift key modulation with non-uniform signaling for visible light communication," in *Proc. 1st IEEE Int. Conf. Commun. China Workshops (ICCC)*, Aug. 2012, pp. 37–42.
[17] R. Singh, T. OFarrell, and J. P. R. David, "An enhanced color shift keying modulation scheme for high-speed wireless visible light communications," *J. Lightw. Technol.*, vol. 32, no. 14, pp. 2582–2592, Jul. 15, 2014.
[18] X. Liang, M. Yuan, J. Wang, Z. Ding, M. Jiang, and C. Zhao, "Constellation design enhancement for color-shift keying modulation of quadrichromatic LEDs in visible light communications," *J. Lightw. Technol.*, vol. 35, no. 17, pp. 3650–3663, Sep. 1, 2017.
[19] L. Jia, J.-Y. Wang, W. Zhang, M. Chen, and J.-B. Wang, "Symbol error rate analysis for colour-shift keying modulation in visible light communication system with RGB light-emitting diodes," *IET Optoelectron.*, vol. 9, no. 5, pp. 199–206, 2015.
[20] J. Tang, L. Zhang, and Z. Wu, "Exact bit error rate analysis for color shift keying modulation," *IEEE Commun. Lett.*, vol. 22, no. 2, pp. 284–287, Feb. 2018.
[21] A. R. Ndjiongue, T. Shongwe, and H. C. Ferreira, "Closed-form BER expressions for HSV-based $M$PSK-CSK systems," *IEEE Commun. Lett.*, vol. 21, no. 5, pp. 1023–1026, May 2017.
[22] A. R. Ndjiongue, T. M. N. Ngatched, and H. C. Ferreira, "APSK-CSK systems based on kite and color wheel constructions," *IEEE Syst. J.*, vol. 13, no. 3, pp. 2396–2407, Sep. 2019.
[23] S. Halawi, E. Yaacoub, S. Kassir, and Z. Dawy, "Performance analysis of circular color shift keying in VLC systems with camera-based receivers," *IEEE Trans. Commun.*, vol. 67, no. 6, pp. 4252–4266, Jun. 2019.
[24] M. A. Atta and A. Bermak, "Channel length modeling for a multiple-input-multiple-output CamCom link," in *Proc. Adv. Wireless Opt. Commun. (RTUWO)*, Nov. 2018, pp. 78–82.
[25] Y. Liu and W. He, "Signal detection and identification in an optical camera communication system in moving state," *J. Phys., Conf. Ser.*, vol. 1873, no. 1, Apr. 2021, Art. no. 012015.
[26] T. Nguyen, N. T. Le, and Y. Min Jang, "Practical design of screen-to-camera based optical camera communication," in *Proc. Int. Conf. Inf. Netw. (ICOIN)*, Jan. 2015, pp. 369–374.
[27] M. A. Atta and A. Bermak, "Accurate channel approximation using perspective projection for a CamCom link," in *Proc. CLEO Pacific Rim Conf.*, Jul. 2018, pp. 1–2.
[28] A. Ashok, M. Gruteser, N. Mandayam, J. Silva, M. Varga, and K. Dana, "Challenge: Mobile optical networks through visual MIMO," in *Proc. 16th Annu. Int. Conf. Mobile Comput. Netw. (MobiCom)*, 2010, pp. 105–112.
[29] T.-C. Bui and S. Kiravittaya, "Demonstration of using camera communication based infrared LED for uplink in indoor visible light communication," in *Proc. IEEE 6th Int. Conf. Commun. Electron. (ICCE)*, Jul. 2016, pp. 71–76.
[30] T. Nguyen, A. Islam, and Y. Min Jang, "Region-of-interest signaling vehicular system using optical camera communications," *IEEE Photon. J.*, vol. 9, no. 1, pp. 1–20, Feb. 2017.

**KE DONG** received the B.S. degree in information engineering and the Ph.D. degree in information and communication system from Xi'an Jiaotong University, China, in 2005 and 2013, respectively. From 2018 to 2019, he was a Visiting Scholar at the EE Department, Columbia University, NY, USA. He is currently a Lecturer with the School of Automation and Information Engineering, Xi'an University of Technology, China. His research interests include optical camera communication and wireless laser communication.

**XIZHENG KE** (Member, IEEE) received the Ph.D. degree from the Chinese Academy of Sciences, in 1996.

He is a Professor and a Doctoral Supervisor with the Xi'an University of Technology. He is a Senior Member of the Chinese Institute of Electronics and China Instrument and Control Society. He has more than ten book publications, 400 academic papers, and 20 patents for invention. His research interests include the wireless laser communication theories and techniques. He received the Outstanding Young Scholar Award from the Chinese Academy of Sciences, in 2000, and the Provincial Awards on Technology Advancement ten times.

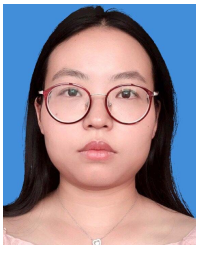

**HUI LI** received the B.S. and M.S. degrees from Xidian University, China, in 2008 and 2012, respectively, and the Ph.D. degree in electromagnetic field and microwave technology from the National Key Laboratory of Antennas and Microwave Technology, Xidian University, in 2018. She is currently a Lecturer with the School of Automation and Information Engineering, Xi'an University of Technology. Her research interests include wideband antennas, reconfigurable antennas, and orbital angular momentum antennas.